analytical chemistry

Article

Cite This: *Anal. Chem.* 2018, 90, 1202−1208

pubs.acs.org/ac

Highly Efficient Electrochemiluminescence of Cyanovinylene-Contained Polymer Dots in Aqueous Medium and Its Application in Imaging Analysis

Yaqiang Feng, Ningning Wang, and Huangxian Ju*

State Key Laboratory of Analytical Chemistry for Life Science, School of Chemistry and Chemical Engineering, Nanjing University, Nanjing 210023, P. R. China

Supporting Information

ABSTRACT: Luminescent semiconducting polymer dots (Pdots) have attracted intense attention in the field of electrochemiluminescence (ECL) due to their nontoxic features. For utilizing the nontoxic Pdots to achieve sensitive ECL bioimaging detection, this work studied the ECL behaviors of poly[2-methoxy-5-(2-ethylhexyloxy)-1,4-(1-cyanovinylene-1,4-phenylene)] (CN-PPV) Pdots in aqueous solution, which introduced an electron-withdrawing cyano group to *p*-phenylenevinylene for enhancing the luminescent efficiency. The CN-PPV Pdots could be both electrochemically oxidized to a positively charged state and electrochemically reduced to a negatively charged state, which led to annihilation of ECL emission. The order of oxidation and reduction greatly influenced the annihilation behavior. In the presence of tri-*n*-propylamine (TPrA) or $S_2O_8^{2-}$ as a coreactant, the CN-PPV Pdots showed strong band gap ECL emission at 602 nm, which followed two different routes and gave ECL efficiencies of 11.22% and 1.84% (vs $Ru(bpy)_3^{2+}$/TPrA), respectively. The high ECL efficiency allowed CN-PPV Pdots/TPrA system for ECL imaging analysis. As a proof-of-methodology, an ECL imaging method was designed via the chelating interaction of metal ions and Pdots to achieve high selectivity. The proposed ECL imaging chip-based sensor exhibited excellent analytical performance for Fe^{3+} with a wide linear range from 100 pM to 100 μM and a detection limit of 67 pM. Compared with the ECL methods based on the direct intensity measurement, the developed ECL imaging method possesses the advantages of simplicity, rapid, and high-throughput and has application potential in monitoring water and food quality.

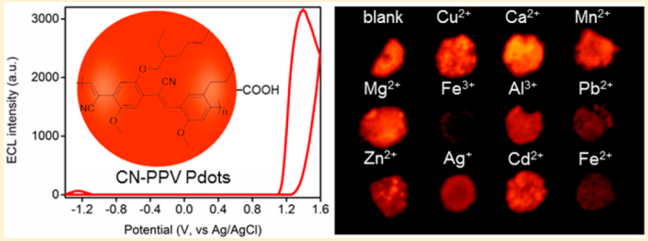

Electrochemiluminescence (ECL) is an electrochemically triggered energy-relaxation process involving electron transfer to form excited states that emit photons.[1−5] Currently, ECL luminophores are divided into three categories: inorganic, organic, and semiconductor nanoparticle systems.[6] Compared with the first two systems, semiconductor nanoparticles, especially quantum dots (QDs), have been widely used in bioanalysis because of their excellent dimensional controllability, surface-trap luminescence, and photostability.[7] However, the presence of heavy metal toxic elements in most QDs, such as CdS,[8] CdSe,[9] CdSe/ZnSe,[10] and PbS QDs,[11,12] limits their biosensing application. Therefore, it is particularly important to develop a novel ECL nanoemitter with good biocompatibility and high ECL efficiency.[13,14]

In recent years, semiconductor polymer dots (Pdots) as a kind of new luminescent nanomaterial[15−20] have been widely used in biosensing,[21,22] in vivo imaging,[23,24] drug and gene delivery,[25,26] single particle tracing,[27,28] and super-resolution imaging.[29] Pdots exhibit excellent optical properties, including extraordinary fluorescence brightness, ultrafast emission rate, and good photostability. Moreover, Pdots show good biocompatibility and tunable optical properties through changing of monomer and easy functionalization.[16] Thus, the ECL behaviors of various Pdots prepared with silole-containing polymer (SCP),[30] poly(9,9-dioctylfluorene-*co*-benzothiadiazole) (PFBT),[31] poly(9,9-dioctylfluorenyl-2,7-diyl) (PFO),[32] poly[2-methoxy-5-(2-ethylhexyloxy)-1,4-phenylenevinylene] (MEH-PPV),[33] and poly[(9,9-di(2-ethylhexyl)-9*H*-fluorene-2,7-vinylene)-*co*-(1-methoxy-4-(2-ethylhe-xyloxy)-2,5-phenylenevinylene)] (PFV)[34] has been reported. Some of these Pdots have even been used for ECL biosensing.[30,32] However, owing to the low ECL efficiency compared to the most frequently inorganic emitters such as $Ru(bpy)_3^{2+}$, these Pdots have not been used for the development of ECL imaging technology yet. To utilize the nontoxic Pdots to achieve sensitive ECL detection and bioimaging, this work studied the ECL behaviors of poly[2-methoxy-5-(2-ethylhexyloxy)-1,4-(1-cyanovinylene-1,4-phenylene)] (CN-PPV, see Figure S1 for molecular structures) Pdots in aqueous solution, which introduced an electron-withdrawing cyano group to the *p*-phenylenevinylene moiety of MEH-PPV for increasing the electron affinity of the polymer and thus enhancing the luminescent efficiency and had already showed the increased fluorescence quantum efficiency (~60%)[35] and 0.68 eV higher ionization potential than those of

Received: September 19, 2017
Accepted: December 8, 2017
Published: December 8, 2017

DOI: 10.1021/acs.analchem.7b03821
Anal. Chem. 2018, 90, 1202−1208

MEH-PPV.[36] The high luminescent efficiency led to strong annihilation ECL emission and sensitive band gap ECL emission in the presence of coreactant, which provided a novel highly efficient emitter for the development of ECL imaging technology.

As a proof-of-methodology, the ECL imaging method could be designed via the chelating interaction of metal ions and the highly luminescent CN-PPV Pdots to achieve the high selectivity using iron(III) cation as a target. As is well-known, iron is the most abundant transition metal in the human body and plays a critical role in various biological process, including metabolism, DNA synthesis, and signal transduction.[37,38] Disruption of iron homeostasis has been linked to disorders such as anemia and hemochromatosis,[37] and excessive iron can cause cancer and neurodegenerative diseases.[38] On the basis of the stable and highly efficient ECL emission of the CN-PPV Pdots/tri-*n*-propylamine (TPrA) system, the proposed ECL imaging method could detect iron(III) in a wide concentration range up to 100 μM and showed a detection limit of 67 pM, which could be used for monitoring of iron ion in water according to the limit of 0.3 mg L^{-1} (5.37 μM), the drinking water standards and health advisories revised by the U.S. Environmental Protection Agency (EPA).[39] Because of its simplicity, rapidity, and high-throughput, the ECL imaging method has significant potential in the analysis of metal ions for monitoring water and food quality.

EXPERIMENTAL SECTION

Materials and Reagents. Poly(styrene-*co*-maleic anhydride) (PSMA) (average M_n: 1700) was purchased from Sigma-Aldrich Co., Ltd. (Shanghai, China). CN-PPV (M_w: 353000, polydispersity: 9.4) was obtained from American Dye Source, Inc. (Quebec, Canada). Carbon crystal paste was purchased from Shanghai Electronic Technology Co., Ltd. Poly Long (Shanghai, China), which was made of superfine carbon powder and low-temperature setting thermoplastic resin. All other reagents were of analytical grade and used as received. Ultrapure water obtained from a Millipore water purification system (≥18 MΩ cm^{-1}, Milli-Q, Millipore) was used in all assays. The ECL measurements were conducted in 0.1 M pH 7.4 PBS containing 0.1 M KNO_3 as the electrolyte.

Apparatus. Transmission electron microscopic (TEM) images were acquired on a JEM-2100 transmission electron microscope (JEOL Ltd., Japan). The TEM samples were prepared by dipping an ultrathin carbon film into 50 μg mL^{-1} of CN-PPV Pdots solution followed by drying in a desiccator. UV−vis absorption spectra were obtained using a Nanodrop-2000C UV−vis spectrophotometer (Thermo, USA). Fluorescence measurements were conducted on an F-7000 fluorescence spectrometer (Hitachi Co., Japan) equipped with a xenon lamp.

ECL experiments were taken using a self-made cell on an MPI-A multifunctional electrochemical and chemiluminescent analytical system (Xi'an Remex Analytical Instrument Co., Ltd. China) with modified glassy carbon electrode (GCE, 5 mm in diameter) as working electrode, platinum wire as counter electrode, and Ag/AgCl electrode (saturated KCl) as the reference electrode. ECL imaging was carried out in a self-build multicolor ECL imaging system equipped with a Retiga R6 color scientific CCD camera (QImaging, Canada) and focus lens (EF 50 mm f/1.2L USM, Canon). The distance between the lens and the ECL chip was adjusted by a mechanical stage. The ECL images were collected by applying a constant potential with a CHI 630B electrochemical workstation (CH Instruments, Shanghai) in a dark box. The ECL spectra were carried out in a CHI 660B electrochemical workstation in conjunction with an F-7000 fluorescence spectrometer using luminescence mode under the closed shutter.

Preparation of CN-PPV Pdots. CN-PPV Pdots were prepared through the nanoprecipitation method by using CN-PPV as a luminescent-conjugated polymer and PSMA as carboxyl-functionalized copolymer.[35] The hydrophobic polystyrene units of PSMA were crimped into the interior of Pdots, and the maleic anhydride units of PMSA were hydrolyzed in water to form carbonxyl groups on the Pdot surface. In brief, 1 mg mL^{-1} of stock solutions of CN-PPV and PSMA in THF were first prepared to obtain the mixture of 50 μg mL^{-1} of CN-PPV and 10 μg mL^{-1} of PSMA. After the mixture was ultrasonically degassed for 20 min at room temperature (Elmasonic P30H, Germany), 2 mL of the mixture was quickly added to 10 mL of water in a bath sonicator (120 W, 37 kHz) for 3 min. The solvent THF was then removed by rotary evaporation under a vacuum followed by filtration through a 0.22 μm poly(ether sulfone) (PES) syringe filter (Millex-GP Filter, Millipore). The carboxyl CN-PPV Pdots were clear and stable for months without obvious aggregation.

Preparation of CN-PPV Pdot-Modified GCE and ECL Characterization. The CN-PPV Pdot-modified GCE was prepared by casting 20 μL of 50 μg mL^{-1} of CN-PPV Pdots solution on a clean GCE and dried at room temperature. The ECL window was placed in front of the photomultiplier tube (PMT, detection range: 300−650 nm). The PMT was set at 600 V for annihilation ECL and 400 V for coreactant ECL. The annihilation ECL curves were obtained by cyclic voltammetric sweep between −1.4 and +1.6 V or multipotential steps at −1.3 V for 1 s and +1.4 V for 1 s with different orders in 0.1 M pH 7.4 PBS. Unless specifically noted, the scan rate was 100 mV s^{-1}.

Preparation of CN-PPV Pdot-Modified Carbon Electrode. The ECL spectra were collected, and ECL imaging was performed on homemade carbon electrodes. The carbon electrode was prepared by spin-coating the carbon crystal paste on indium tin oxide (ITO) at 4000 rpm for 10 s and drying at 60 °C. The CN-PPV Pdot-modified carbon electrode was prepared for collecting the ECL spectra by casting 20 μL of 50 μg mL^{-1} of CN-PPV Pdot solution on the carbon surface and dried at room temperature. The ECL imaging chip (25 × 25 mm) was constructed by pasting a layer of sticker with 3 × 4 well array (diameter: 2 mm, depth: 1 mm) on the carbon surface and a rubber ring on the sticker to fix a platinum wire and a Ag/AgCl wire as the counter and reference electrodes (Figure S2). The wells were then modified by casting different mixtures containing CN-PPV Pdots and dried at room temperature.

ECL Quantum Efficiency. The ECL quantum efficiency is defined as the number ratio of emitted photons to annihilated radical luminophores. Because of the experimental difficulty in measuring the absolute efficiency, relative ECL efficiency is usually calculated using the equation[40]

$$\Phi_{ECL} = \Phi^{\circ}_{ECL}(I/Q)/(I^{\circ}/Q^{\circ}) \quad (1)$$

where Φ_{ECL} and Φ°_{ECL} are the ECL efficiency, I and I° are the integrated ECL intensities (integrating ECL spectrum vs wavelength), and Q and Q° are the consumed charges (integrating current vs time) of the sample and standard, respectively. Here, the ECL spectrum of 1 mM $Ru(bpy)_3^{2+}$-

DOI: 10.1021/acs.analchem.7b03821
Anal. Chem. 2018, 90, 1202−1208

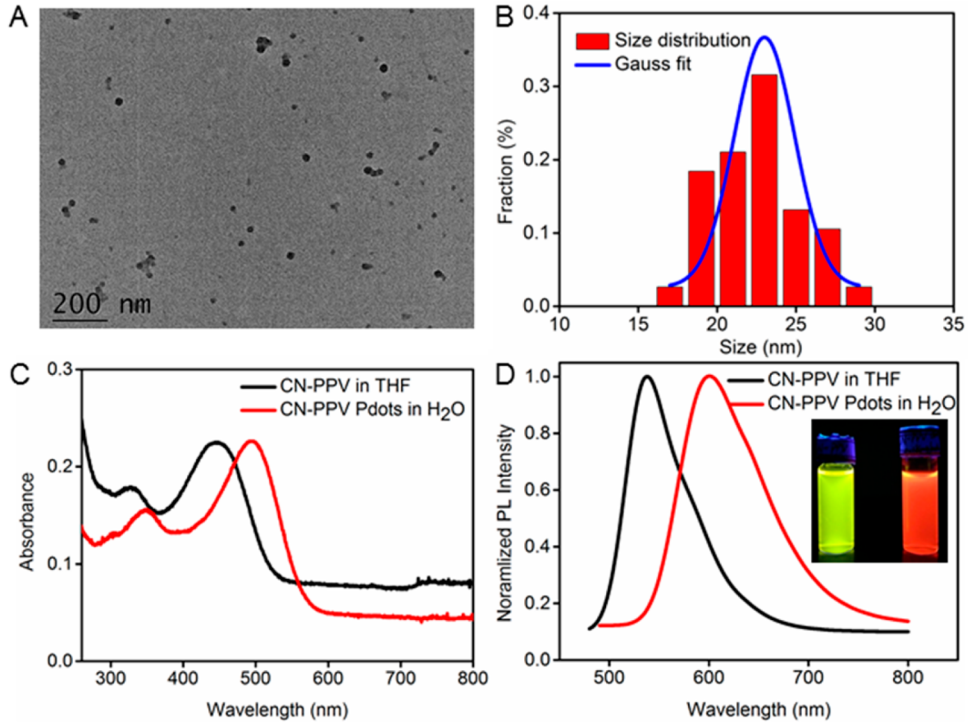

Figure 1. (A) TEM image and (B) size distribution of CN-PPV Pdots. (C) UV−vis absorption and (D) fluorescence spectra of CN-PPV in THF and CN-PPV Pdots in H_2O. The excitation wavelengths for CN-PPV and CN-PPV Pdots are 445 and 494 nm, respectively. (D, inset) Photograph of CN-PPV in THF (left) and CN-PPV Pdots in water (right) under UV irradiation at 365 nm.

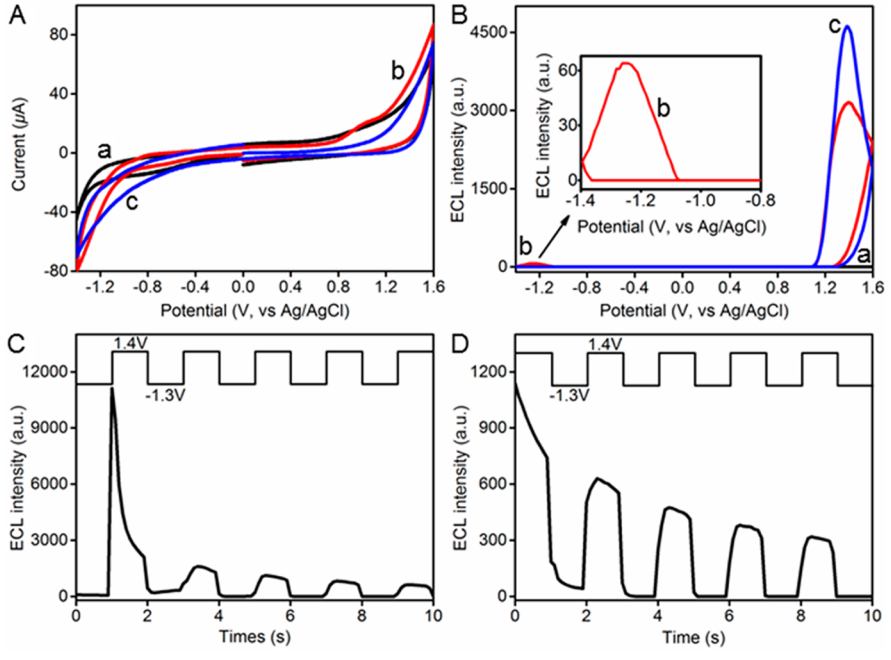

Figure 2. (A) CV and (B) ECL curves of bare (a) and CN-PPV Pdot-modified (b, c) GCE in nitrogen-saturated 0.1 M pH 7.4 PBS from 0 to −1.4 to +1.6 V (b) and 0 to +1.6 to −1.4 V (c) at 100 mV s^{-1}. (C,D) ECL transients of CN-PPV Pdot-modified GCE in the nitrogen-saturated 0.1 M pH 7.4 PBS by multipotential steps of 1 s at −1.3 and then +1.4 V (C) and +1.4 and then −1.3 V (D). PMT: 600 V.

modified carbon electrode with the Φ°_{ECL} value of 1 was used as the standard, which was obtained by applying a constant potential of +1.2 V in 0.1 M pH 7.4 PBS containing 0.1 M TPrA for 9 s. The anodic and cathodic ECL spectra of CN-PPV Pdot-modified carbon electrode were recorded in 0.1 M pH 7.4 PBS containing 0.1 M TPrA or $S_2O_8^{2-}$ as coreactant at +1.4 V and −1.3 V for 9 s, respectively.

ECL Imaging Detection of Iron Ion. The quenching effects of 11 kinds of metal ions on ECL emission of CN-PPV Pdots were investigated by mixing 5 μg mL^{-1} of CN-PPV Pdots with 1 mM metal ions, such as Cu^{2+}, Ca^{2+}, Mn^{2+}, Mg^{2+}, Fe^{3+}, Al^{3+}, Pb^{2+}, Zn^{2+}, Ag^{+}, Cd^{2+}, and Fe^{2+}, or various concentrations of Fe^{3+} in aqueous solution, and then dropping 2 μL of these mixed solutions into the exposed wells of the ECL chip to be

DOI: 10.1021/acs.analchem.7b03821
Anal. Chem. 2018, 90, 1202−1208

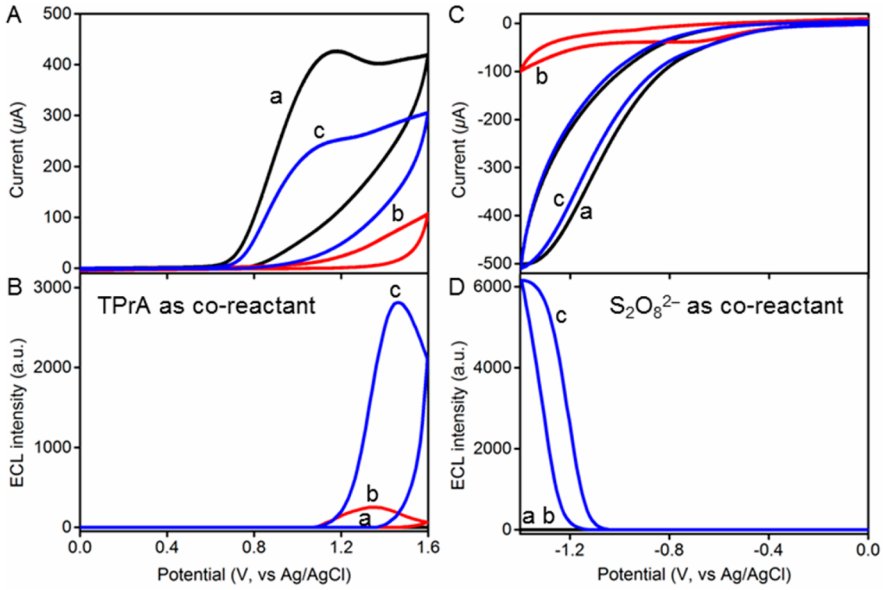

Figure 3. (A,C) CV and (B,D) ECL curves of bare (a) and CN-PPV Pdot-modified (b,c) GCE in 0.1 M pH 7.4 PBS in the absence (b) and presence (a,c) of (A,B) 10 mM TPrA as anodic coreactant or (C,D) 10 mM $S_2O_8^{2-}$ as cathodic coreactant. Scan rate: 100 mV s^{-1}. PMT: 400 V.

dried at 60 °C, respectively. The ECL imaging detection was carried out in 0.1 M pH 7.4 PBS containing 30 mM TPrA solution.

RESULTS AND DISCUSSION

Characterization of CN-PPV Pdots. The carboxyl CN-PPV Pdots were prepared with CN-PPV and PSMA polymers by nanoprecipitation method. PSMA polymer brought about the carboxyl groups on the Pdot surface by hydrolysis of maleic anhydride.[35] The TEM image of the CN-PPV Pdots showed an essential spherical morphology and monodisperse feature with a relatively narrow Gauss size distribution ranging from 15 to 30 nm and an average diameter of 22.3 nm (Figure 1). The UV−vis absorption spectrum of CN-PPV Pdots solution showed two absorption peaks at 347 and 494 nm, which exhibited significant red-shift as compared to those of CN-PPV in THF (Figure 1C). The fluorescence spectrum of the CN-PPV Pdot solution showed an emission peak at 600 nm, which also exhibited an obvious red-shift by 60 nm compared with that of CN-PPV in THF (Figure 1D). Under UV lamp illumination at 365 nm, the CN-PPV Pdots in water emitted reddish-brown fluorescence, whereas CN-PPV in THF emitted bright yellow fluorescence (inset in Figure 1D). The red-shift could be attributed to the increasing interchain interaction due to the chain collapse.[16]

Annihilation ECL Behaviors of CN-PPV Pdots. In the nitrogen-saturated 0.1 M pH 7.4 PBS, the cyclic voltammogram of bare GCE did not show an obvious response, whereas the CN-PPV Pdot-modified electrode showed an irreversible anodic peak at +1.0 V and higher reduction current than bare GCE at potentials more negative than −0.9 V (Figure 2A, curves a and b), indicating the oxidation or reduction of CN-PPV Pdots through injecting the holes or electrons into the CN-PPV Pdots, which led to a strong annihilation ECL emission in the anodic region with an ECL peak at +1.4 V and a relatively weak annihilation ECL emission in the cathodic region with a peak at −1.25 V (Figure 2B, curve b). However, these phenomena were only observed when the potential was scanned cathodically from 0 to −1.4 V and then anodically from −1.4 to +1.6 V, and the cathodic ECL emission was undetectable when the potential was first scanned from 0 to +1.6 V and then to −1.4 V (Figure 2B, curve c), indicating more stable electroreduced forms of Pdots.[9]

The annihilation ECL activity and relative stability of the free radicals were further studied with ECL transient technology by alternately switching the electrode potential at +1.4 and −1.3 V for 1 s to achieve the oxidation and reduction of CN-PPV Pdots, respectively. When the potential started at −1.3 V and alternately stepped from −1.3 and +1.4 V, no ECL emission was observed at −1.3 V, and an obvious sharp and intensive ECL emission was generated following the annihilation mechanism (eqs 2−5) (Figure 2C). The ECL emission quickly decreased at +1.4 V and showed very low intensity in the followed potential steps from −1.3 and +1.4 V. These phenomena confirmed the stable reduced form of CN-PPV Pdots.

$$\text{Pdots (film)} + e^- \rightarrow \text{Pdotso}^{\bullet -}\text{ (film)} \quad (2)$$

$$\text{Pdots (film)} - e^- \rightarrow \text{Pdotso}^{\bullet +}\text{ (film)} \quad (3)$$

$$\text{Pdots}^{\bullet +}\text{ (film)} - \text{Pdots}^{\bullet -}\text{ (film)} \rightarrow \text{Pdotso}^{*}\text{ (film)} \quad (4)$$

$$\text{Pdots}^{*}\text{ (film)} \rightarrow \text{Pdots (film)} + h\nu \quad (5)$$

On the contrary, when the potential started at +1.4 V and alternately stepped from +1.4 V and −1.3 V, an intensive ECL emission with relatively lower intensity could be observed at the starting potential (Figure 2D), which was called preannihilation process and also observed in the study of CdSe nanocrystals in organic solution.[9] This might be due to the reaction of the oxidative state of CN-PPV Pdots with the trace amount of OH^- in water acting as an electron donor to produce light emission.[30] In the followed stepping from +1.4 V and −1.3 V, no ECL emission was observed, and the ECL emission occurred again at the stepping from −1.3 V and +1.4 V, further demonstrating the stable reduced form.

Coreactant ECL Behaviors of CN-PPV Pdots. In the presence of TPrA, strong anodic ECL emission of CN-PPV Pdot-modified GCE could be detected at +1.46 V in 0.1 M pH

DOI: 10.1021/acs.analchem.7b03821
Anal. Chem. 2018, 90, 1202−1208

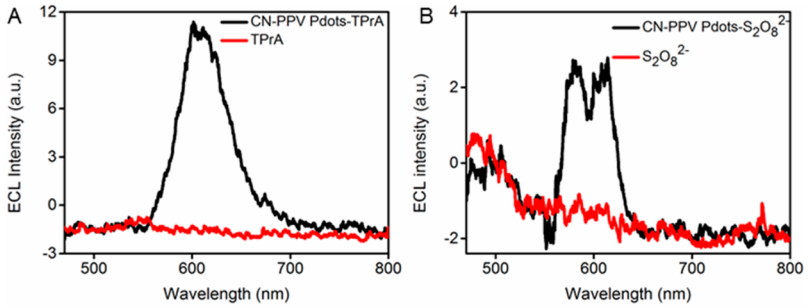

Figure 4. ECL spectra of bare and CN-PPV Pdot-modified carbon electrode in 0.1 M pH 7.4 PBS containing (A) 0.1 M TPrA as anodic and (B) 0.1 M $S_2O_8^{2-}$ as cathodic coreactant at +1.4 and −1.3 V.

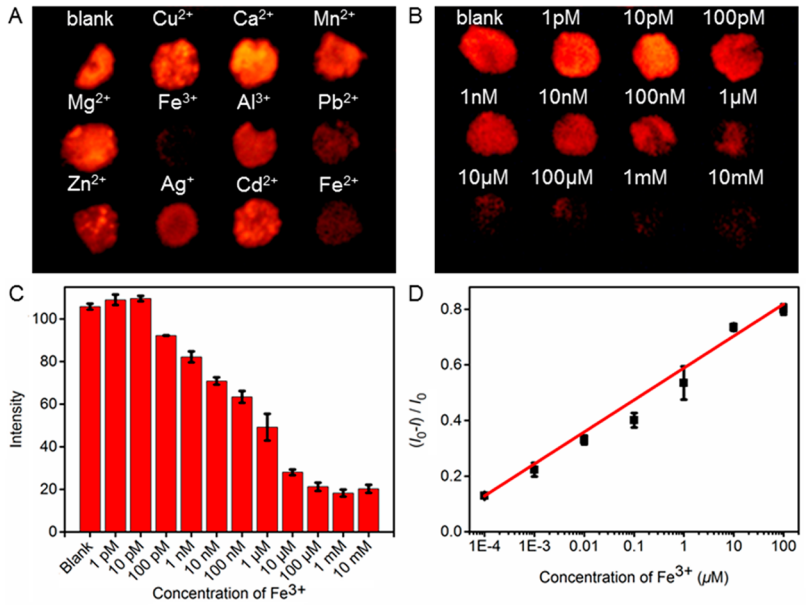

Figure 5. ECL imaging of CN-PPV Pdots at the carbon electrode in the presence of (A) various metal ions (1 mM) and (B) Fe^{3+} at different concentrations at +1.4 V. (C) Dependence of ECL intensity on Fe^{3+} concentration and (D) calibration curve.

7.4 PBS with a PMT set voltage of 400 V along with an irreversible oxidation peak of TPrA at +1.17 V (Figure 3A and B, curve c). The small ECL emission at +1.35 V in the absence of TPrA (Figure 3B, curve b) could be attributed to the annihilation ECL due to the trace amount of OH^- as electron donor in water,[30] whereas the much stronger anodic ECL peak (Figure 3B, curve c) resulted from the coreactant ECL emission. The ECL intensity of the CN-PPV Pdots/TPrA system was 11.3-times higher than that in the absence of TPrA. The oxidation of TPrA produced a strong reducing agent, $TPrA^{\bullet}$, which injected electrons into the oxidized CN-PPV Pdots, $Pdots^{\bullet+}$, to produce the excited state Pdots*. The anodic ECL mechanism was proposed as eqs 6−10)

$$Pdots - e^- \rightarrow Pdots^{\bullet+} \quad (6)$$

$$TPrA - e^- \rightarrow TPrAH^{\bullet+} \quad (7)$$

$$TPrAH^{\bullet+} - H^+ \rightarrow TPrA^{\bullet} \quad (8)$$

$$Pdots^{\bullet+} + TPrA^{\bullet} \rightarrow Pdots^* + Pr_2N^+HC{=}CH_2CH_3 \quad (9)$$

$$Pdots^* \rightarrow Pdots + h\nu \quad (10)$$

The CN-PPV Pdot-modified GCE also showed an obvious cathodic ECL emission at −1.38 V in the presence of $S_2O_8^{2-}$ as cathodic coreactant along with the reduction of $S_2O_8^{2-}$ (Figure 3C and D). No ECL could be observed at bare GCE or in the absence of $S_2O_8^{2-}$ (Figure 3D, curves a and b). The cathodic response of 10 mM $S_2O_8^{2-}$ at CN-PPV Pdot-modified GCE was almost the same as that observed at bare GCE (Figure 3C, curves a and c). The corresponding ECL mechanism of CN-PPV Pdots/$S_2O_8^{2-}$ system could be described as

$$Pdots + e^- \rightarrow Pdots^{\bullet-} \quad (11)$$

$$S_2O_8^{2-} + e^- \rightarrow SO_4^{\bullet-} + SO_4^{2-} \quad (12)$$

$$Pdots^{\bullet-} + SO_4^{\bullet-} \rightarrow Pdots^* + SO_4^{2-} \quad (13)$$

$$Pdots^* \rightarrow Pdots + h\nu \quad (14)$$

ECL Efficiency. The ECL spectrum of the CN-PPV Pdot-modified carbon electrode at +1.4 V in 0.1 M pH 7.4 PBS containing TPrA showed a peak at the wavelength of 602 nm (Figure 4A), which was consistent with the fluorescence emission peak of CN-PPV Pdots in H_2O (600 nm, Figure 1D), indicating the same excited species (eq 10). Thus, the ECL emission originated from the band gap emission of CN-PPV Pdots. Because of the same excited species in both annihilation and coreactant ECL emission, the ECL band gap could be estimated from the onset potentials of anodic and cathodic annihilation ECL emission at +1.1 and −1.08 V to be 2.08 eV

DOI: 10.1021/acs.analchem.7b03821
Anal. Chem. 2018, 90, 1202−1208

(Figure 2B, red curve), which was consistent with the optical band gap of 2.07 eV. The latter was obtained from the equation E_S (eV) = 1239.8/λ (nm) and the wavelength of 600 nm (Figure 1D, red curve).

Similarly, the cathodic ECL emission of the CN-PPV Pdot-modified carbon electrode in the presence of $S_2O_8^{2-}$ occurred at the wavelength ranging from 550 to 650 nm (Figure 4B), which showed two split peaks, and the anodic ECL emission peak of the $Ru(bpy)_3^{2+}$/TPrA system occurred at 609 nm (Figure S3). From eq 1, the integrated ECL intensities and consumed charges, the relative ECL efficiency of CN-PPV Pdots/TPrA system, and CN-PPV Pdots/$S_2O_8^{2-}$ system were calculated to be 11.22% and 1.84% (vs $Ru(bpy)_3^{2+}$/TPrA). The former was 8.63-times higher than that of 1.3% for the PFV Pdots/TPrA system.[34] The highly efficient ECL emission of the CN-PPV Pdot-modified carbon electrode in the presence of TPrA allowed its potential application in ECL imaging analysis.

ECL Imaging Detection of Iron Ion. The cyano group in CN-PPV and carboxyl in PSMA could be used as selective coordination groups of metal ions for chelating interaction of the CN-PPV Pdots and metal ions, which changed the ECL response to provide a signal switch for detection of metal ions. From the results described above, the CN-PPV Pdots showed both strong annihilation ECL in nitrogen-saturated solution and coreactant-based ECL emission in the presence of TPrA as anodic or $S_2O_8^{2-}$ as cathodic coreactant. Considering the need for nitrogen-saturated detection solution for obtaining annihilation ECL (Figure 2B), the quick attenuation of anodic annihilation ECL at +1.4 V (Figure 2C), which was adverse for imaging analysis, and 11.3-times higher ECL intensity of CN-PPV Pdots/TPrA system than anodic annihilation ECL (Figure 3B), the coreactant-based CN-PPV Pdots/TPrA system with high ECL efficiency was used for obtaining the high-quality ECL image for imaging analysis.

After the mixtures of CN-PPV Pdots and metal ions were coated on each exposed carbon well of the chip, respectively, the ECL images of these metal ions were conducted in 0.1 M pH 7.4 PBS containing 10 mM TPrA. As shown in Figure 5A, the reddish-brown ECL emission of CN-PPV Pdots could be quenched by Fe^{3+}, Pb^{2+}, Zn^{2+}, Ag^{+}, and Fe^{2+}, whereas other metal ions such as Cu^{2+}, Ca^{2+}, Mn^{2+}, Mg^{2+}, and Cd^{2+} did not show an obvious effect on the ECL emission of CN-PPV Pdots. This quenching phenomenon was different from the aggregation-induced fluorescence quenching of carboxyl PFBT Pdots by both Cu^{2+} and Fe^{2+} due to the chelating interactions between carboxyl groups on the Pdot surface and metal ions.[41] Here, the strong chelating ability of the cyano group in CN-PPV with metal ions, such as Fe^{2+} and Fe^{3+} with cumulative stability constants of 35 and 42, respectively,[42] led to the electron-transfer quenching from the electrogenerated Pdots* to the chelated metal ions.[43] The quenching efficiency of Fe^{3+} was the maximum among these ions at the same concentration. At the concentration of 1 mM, the quenching efficiency was 83%, which gradually decreased with the decrease of Fe^{3+} concentration (Figure 5B and C), and showed a linear relationship between $(I_0 - I)/I_0$ and the logarithm of Fe^{3+} concentration ranging from 100 pM to 100 μM with the correlation coefficient R of 0.997 (Figure 5D), where I_0 and I were the ECL intensities in the absence or presence of Fe^{3+} at a given concentration. The regression equation was $(I_0 - I)/I_0 = 0.589 \times \log C\ (Fe^{3+}) + 0.115$. The limit of detection was 67 pM at a signal-to-noise ratio of 3, which was significantly lower than that of Pdot-based fluorescence sensors.[41] Obviously, the relatively weaker quenching efficiencies of Pb^{2+}, Zn^{2+}, Ag^{+}, and Fe^{2+} might interfere with the detection of Fe^{3+}. However, these interfering ions could be first covered for practical ECL imaging application by adding general masking agents in the mixture. The addition of ethylenediaminetetraacetic acid (EDTA) could almost completely recover the ECL quenched by Pb^{2+}, Zn^{2+}, Ag^{+}, and Fe^{2+} due to the strong chelating effect of EDTA (Figure S4). Thus, this ECL chip-based imaging detection method not only possessed high sensitivity and wide detectable concentration range but also could achieve rapid and high-throughput analysis of Fe^{3+} ion, which extended the ECL application of Pdots.

CONCLUSIONS

This work systematically studies the ECL behaviors of Pdots in aqueous solution, including the annihilation and coreactant ECL emission, which possesses the same excited species as the photoluminescence. The introduction of electron-withdrawing cyano group to *p*-phenylenevinylene moiety of MEH-PPV efficiently increases the luminescent efficiency and enhances the ECL intensity. A strong annihilation ECL emission is observed in the anodic region due to the relatively stable electroreduced forms of Pdots. The much stronger ECL emission can be obtained in the presence of TPrA or $S_2O_8^{2-}$ as anodic or cathodic coreactant, indicating a new emitter for ECL imaging analysis. Thus, an ECL imaging method has been designed via the chelating interaction of metal ions and Pdots to achieve the selectivity analysis, which exhibits excellent analytical performance with high sensitivity and a wide detectable concentration range. Compared with the traditional ECL analysis, this ECL imaging method features the advantages of simplicity, rapidity, and high-throughput and thus extends the ECL application of Pdots.

ASSOCIATED CONTENT

Supporting Information

The Supporting Information is available free of charge on the ACS Publications website at DOI: 10.1021/acs.analchem.7b03821.

Molecular structure of CN-PPV, photograph of ECL imaging chip, ECL spectrum of $Ru(bpy)_3^{2+}$/TPrA system, and ECL imaging of metal ions in the presence of EDTA (PDF)

AUTHOR INFORMATION

Corresponding Author

*Phone/Fax: +86-25-89683593. E-mail: hxju@nju.edu.cn.

ORCID

Huangxian Ju: 0000-0002-6741-5302

Notes

The authors declare no competing financial interest.

ACKNOWLEDGMENTS

This work was supported by National Natural Science Foundation of China (21635005, 21361162002) and the program B for outstanding Ph.D. candidate of Nanjing University.

REFERENCES

(1) Bard, A. J. *Electrogenerated Chemiluminescence*; Marcel Dekker: New York, 2004.

DOI: 10.1021/acs.analchem.7b03821
Anal. Chem. 2018, 90, 1202−1208

(2) Miao, W. J. *Chem. Rev.* **2008**, *108*, 2506−2553.
(3) Lei, J. P.; Ju, H. X. *TrAC, Trends Anal. Chem.* **2011**, *30*, 1351−1359.
(4) Zhao, W. W.; Wang, J.; Zhu, Y. C.; Xu, J. J.; Chen, H. Y. *Anal. Chem.* **2015**, *87*, 9520−9531.
(5) Liu, Z. F.; Qi, W. J.; Xu, G. B. *Chem. Soc. Rev.* **2015**, *44*, 3117−3142.
(6) Hu, L. Z.; Xu, G. B. *Chem. Soc. Rev.* **2010**, *39*, 3275−3304.
(7) Howes, P. D.; Chandrawati, R.; Stevens, M. M. *Science* **2014**, *346*, 1247390.
(8) Ren, T.; Zhou, J. Z.; Tu, Y. F.; Xu, S.; Zhu, J. J. *Electrochem. Commun.* **2005**, *7*, 5−9.
(9) Myung, N.; Ding, Z. F.; Bard, A. J. *Nano Lett.* **2002**, *2*, 1315−1319.
(10) Myung, N.; Bae, Y.; Bard, A. J. *Nano Lett.* **2003**, *3*, 1053−1055.
(11) Sun, L.; Bao, L.; Hyun, B. R.; Bartnik, A. C.; Zhong, Y. W.; Reed, J. C.; Pang, D. W.; Abruna, H. D.; Malliaras, G. G.; Wise, F. W. *Nano Lett.* **2009**, *9*, 789−793.
(12) Hesari, M.; Swanick, K. N.; Lu, J. S.; Whyte, R.; Wang, S.; Ding, Z. F. *J. Am. Chem. Soc.* **2015**, *137*, 11266−11269.
(13) Zheng, L. Y.; Chi, Y. W.; Dong, Y. Q.; Lin, J. P.; Wang, B. B. *J. Am. Chem. Soc.* **2009**, *131*, 4564−4565.
(14) Cheng, C. M.; Huang, Y.; Wang, J.; Zheng, B. Z.; Yuan, H. Y.; Xiao, D. *Anal. Chem.* **2013**, *85*, 2601−2605.
(15) Pecher, J.; Mecking, S. *Chem. Rev.* **2010**, *110*, 6260−6279.
(16) Wu, C.; Chiu, D. T. *Angew. Chem., Int. Ed.* **2013**, *52*, 3086−3109.
(17) Feng, L.; Zhu, C.; Yuan, H.; Liu, L.; Lv, F.; Wang, S. *Chem. Soc. Rev.* **2013**, *42*, 6620−6633.
(18) Peng, H. S.; Chiu, D. T. *Chem. Soc. Rev.* **2015**, *44*, 4699−4722.
(19) Jiang, Y.; McNeill, J. *Chem. Rev.* **2017**, *117*, 838−859.
(20) Yu, J.; Rong, Y.; Kuo, C. T.; Zhou, X. H.; Chiu, D. T. *Anal. Chem.* **2017**, *89*, 42−56.
(21) Cordovilla, C.; Swager, T. M. *J. Am. Chem. Soc.* **2012**, *134*, 6932−6935.
(22) Li, P.; Liu, L.; Xiao, H.; Zhang, W.; Wang, L.; Tang, B. *J. Am. Chem. Soc.* **2016**, *138*, 2893−2896.
(23) Pu, K.; Shuhendler, A. J.; Jokerst, J. V.; Mei, J.; Gambhir, S. S.; Bao, Z.; Rao, J. *Nat. Nanotechnol.* **2014**, *9*, 233−239.
(24) Shuhendler, A. J.; Pu, K.; Cui, L.; Uetrecht, J.; Rao, J. *Nat. Biotechnol.* **2014**, *32*, 373−380.
(25) Feng, X.; Lv, F.; Liu, L.; Tang, H.; Xing, C.; Yang, Q.; Wang, S. *ACS Appl. Mater. Interfaces* **2010**, *2*, 2429−2435.
(26) Moon, J. H.; Mendez, E.; Kim, Y.; Kaur, A. *Chem. Commun.* **2011**, *47*, 8370−8372.
(27) Yu, J.; Wu, C.; Sahu, S. P.; Fernando, L. P.; Szymanski, C.; McNeill, J. *J. Am. Chem. Soc.* **2009**, *131*, 18410−18414.
(28) Liu, Z.; Yang, Y.; Sun, Z.; Wu, C. *Opt. Mater.* **2016**, *62*, 1−6.
(29) Chen, X.; Liu, Z.; Li, R.; Shan, C.; Zeng, Z.; Xue, B.; Yuan, W.; Mo, C.; Xi, P.; Wu, C.; Sun, Y. *ACS Nano* **2017**, *11*, 8084−8091.
(30) Feng, Y. Q.; Dai, C. H.; Lei, J. P.; Ju, H. X.; Cheng, Y. X. *Anal. Chem.* **2016**, *88*, 845−850.
(31) Chang, Y. L.; Palacios, R. E.; Fan, F. R. F.; Bard, A. J.; Barbara, P. F. *J. Am. Chem. Soc.* **2008**, *130*, 8906−8907.
(32) Lu, Q.; Zhang, J.; Wu, Y.; Chen, S. *RSC Adv.* **2015**, *5*, 63650−63654.
(33) Dai, R. P.; Wu, F. M.; Xu, H. F.; Chi, Y. W. *ACS Appl. Mater. Interfaces* **2015**, *7*, 15160−15167.
(34) Wu, F.; Feng, Y.; Chi, Y. *J. Electroanal. Chem.* **2016**, *779*, 47−54.
(35) Ye, M.; Wu, C.; Jin, W.; Wang, M.; Chan, Y. H.; Yu, J.; Sun, W.; Hayden, S.; Chiu, D. T. *Chem. Commun.* **2012**, *48*, 1778−1780.
(36) Li, Y.; Cao, Y.; Gao, J.; Wang, D.; Yu, G.; Heeger, A. J. *Synth. Met.* **1999**, *99*, 243−248.
(37) Carter, K. P.; Young, A. M.; Palmer, A. E. *Chem. Rev.* **2014**, *114*, 4564−4601.
(38) Hirayama, T.; Nagasawa, H. *J. Clin. Biochem. Nutr.* **2017**, *60*, 39−48.
(39) United States Environmental Protection Agency, EPA. 2009 edition of the drinking water standards and health advisories, EPA 822-R-09-011 http://www.epa.gov/waterscience/criteria/drinking/dwstandards2009.pdf (accessed Nov. 03, 2010).
(40) Hesari, M.; Workentin, M. S.; Ding, Z. *ACS Nano* **2014**, *8*, 8543−8553.
(41) Chan, Y. H.; Jin, Y.; Wu, C.; Chiu, D. *Chem. Commun.* **2011**, *47*, 2820−2822.
(42) Speight, J. G.. *Lange's Handbook of Chemistry*, 16th; McGraw-Hill Companies: New York, 2005; P1.359.
(43) Fan, C.; Plaxco, K. W.; Heeger, A. J. *J. Am. Chem. Soc.* **2002**, *124*, 5642−5643.

DOI: 10.1021/acs.analchem.7b03821
Anal. Chem. 2018, 90, 1202−1208